arXiv:1603.00764v1 [math.AP] 2 Mar 2016

TOWARDS MONITORING CRITICAL MICROSCOPIC PARAMETERS FOR ELECTROPERMEABILIZATION

H. AMMARI, T. WIDLAK, AND W. ZHANG

Abstract. Electropermeabilization is a clinical technique in cancer treatment to locally stimulate the cell metabolism. It is based on electrical fields that change the properties of the cell membrane. With that, cancer treatment can reach the cell more easily. Electropermeabilization occurs only with accurate dosage of the electrical field. For applications, a monitoring for the amount of electropermeabilization is needed. It is a first step to image the macroscopic electrical field during the process. Nevertheless, this is not complete, because electropermeabilization depends on critical individual properties of the cells such as their curvature. From the macroscopic field, one cannot directly infer that microscopic state. In this article, we study effective parameters in a homogenization model as the next step to monitor the microscopic properties in clinical practice. We start from a physiological cell model for electropermeabilization and analyze its well-posedness. For a dynamical homogenization scheme, we prove convergence and then analyze the effective parameters, which can be found by macroscopic imaging methods. We demonstrate numerically the sensitivity of these effective parameters to critical microscopic parameters governing electropermeabilization. This opens the door to solve the inverse problem of rreconstructing these parameters.

Mathematics Subject Classification (MSC2000): 35B30, 35R30.

Keywords: electropermeabilization, cell membrane, homogenization, sensitivity of effective parameters.

1. Introduction

The technique of electropermeabilization (formerly referred to as electroporation) is employed to make the chemotherapeutical treatment of cancer more efficient and avoid side-effects. Instead of spreading out drugs over the whole body, electropermeabilization makes it possible to focus drug application on special areas. The mechanism of electropermeabilization relies on careful exposition of biological tissue to electrical fields: this changes the membrane properties of the cells such that treatment can enter more easily just at precisely defined areas of the tissue [6, 12].

The local change in microscopic tissue properties, which electropermeabilization effects, occurs only with field strengths above a certain threshold. On the other hand, too strong fields result in cell death. One therefore thinks of electropermeabilization occurring within a certain threshold of intensity of the local electric field [4].

For treatment planning in electropermeabilization, one is interested in the percentage of electroporated cells over the whole tissue to form decisions in the short term how to gear treatment [10, 4, 12].

This work was supported by the ERC Advanced Grant Project MULTIMOD–267184.

One would like supervise the electropermeabilization using measurements of the electric field distribution with image modalities like in [10]. In that work, measurements of magnetic resonance electrical impedance tomography [19] have been employed to find the electrical field distribution. A threshold is then applied to find the electroporated cells.

Yet this approach is only the first step in a larger program:

- the electrical field distribution reconstructed by an imaging modality is a macroscopic quantity;
- the thresholding hypothesis is a simplification and should be refined [4];
- the minimum transmembrane voltage governing electropermeabilization is determined by specific cell characteristics like the curvature of the cell membrane [21].

One solution to find about microscopic parameters from measurements is to take general models and do a specific parameter fitting with preselected cells like in [4]. In clinical practice, though, a preselected cell population may be unavailable for the analysis.

In this paper, we tackle the next step in electropermeabilization monitoring and investigate the question to determine microscopic parameters from macroscopic measurements. The modelling used stems from general physiological tissue models for cells, asymptotically simplified by Neu and Krassowska [14]. Whereas the mathematical well-posedness of the model of that model is not available in the literature, there exists an investigation of well-posedness for a similar model in [8]. In this paper, demonstrate the local well-posedness of the asymptotic cell model of [14], as well as the absence of a blow up. A variant of the model is shown to be globally well-posed.

In order to describe the relation between macroscopic and microscopic quantities, we apply the homogenization scheme in [2] to the cell model of Neu and Krassowska [14]. This not only describes isotropic effective parameters such as classical theory [16], but includes also anisotropy. We provide a convergence analysis for the homogenized solution.

Then we study numerically the sensitivity of the effective parameters to:

- the conductivities of the extra- and intracellular media;
- the shape of the cell membrane;
- the volume fraction of the cells;
- the lattice structure of the cells.

We refer to research in [21, 7, 11, 15, 18], where these critical parameters for electropermeabilization have been investigated, partly from an empirical or computer simulation point of view.

The structure of the paper is as follows. In Section 2, we introduce the model of [14] on the cellular scale. In Section 3, we investigate its well-posedness properties. In Section 4, we perform the homogenization and show the convergence of the homogenized solution. In Section 5, we provide a sensitivity analysis of the effective parameters, showing dependence on microscopic properties, summarized in Table 2. A discussion and final remarks in Section 6 conclude the article.

2. Modelling electropermeabilization on the cellular scale

2.1. **Membrane model.** Let $Y \Subset \mathbb{R}^d$ be a bounded domain representing the cell, and let $\Gamma \subset Y$ be the membrane of the cell. Let

$$Y \setminus \Gamma = Y_i \cup Y_e,$$

where Y_i (resp. Y_e) is be the inner (resp. the outer) domain. Let $\sigma_i(x)$ be the conductivity of the cell domain Y_i, and $\sigma_e(x)$ be the conductivity outside the cells on Y_e.

Let u_0 be an imposed voltage on the boundary of Y. An electrostatic model for the electrical field $u(x,t)$ on Y in the inner and outer domain is

$$\nabla \cdot (\sigma(x)\, \nabla u(x,t)) = 0 \qquad \text{on } Y \setminus \Gamma = Y_i \cup Y_e, \tag{1}$$

$$u = u_0 \qquad \text{on } \partial Y, \text{ with } \Delta u_0 = 0 \text{ in } Y, \tag{2}$$

$$\sigma_e \mathbf{n} \cdot \nabla u^+ = \sigma_i \mathbf{n} \cdot \nabla u^- = \sigma \mathbf{n} \cdot \nabla u = \sigma \partial_n u \qquad \text{on } \Gamma. \tag{3}$$

Here and throughout this paper, ∂_n denotes the normal derivative.

2.2. **Electropermeabilization models.** In addition to the membrane model, a time-varying conductivity $\sigma_m(x,t)$ for $x \in \Gamma$ is taken account of. The general effect of electropermeabilization is described by relating σ_m and the membrane thickness δ to the transmembrane potential (TMP) jump $u^+(x,t) - u^-(x,t) := [u](x,t)$ in an ordinary differential equation (ODE) on Γ:

$$\sigma(x)\mathbf{n} \cdot \nabla u(x,t) = \frac{c_m}{\delta} \partial_t [u](x,t) + \frac{\sigma_m\left([u](x,t),t\right)}{\delta} [u](x,t) \qquad \text{on } \Gamma. \tag{4}$$

Here, the vector $\mathbf{n}$ is the outward normal to Γ, ∂_n is the normal derivative, the superscripts $\pm$ denote the limits for outside and inside Y_i, and c_m is a positive constant.

The membrane conductivity σ_m in (4) is described by different models. In [7], Mir et al. propose a static model based on

$$\sigma_m([u]) = \sigma_{m0} + K\ (e^{\beta[u]} - 1), \tag{5}$$

for some constants σ_{m0}, K, and β, and used the model (1)-(4) and (5) as a boundary-value problem for an elliptic equation with nonlinear transmission conditions at the membrane.

The classical and more involved model for σ_m due to Neu and Krassowska [14] is explained in the following. It assumes that σ_m is the sum of σ_{m0} and an electropermeabilization current. The latter is proportional to the pore density N, which in turn is governed by an ordinary differential equation:

$$\sigma_m([u],t) = \sigma_{m0} + \beta N([u],t) \qquad \text{on } \Gamma\times]0,T[, \tag{6}$$

$$N([u],0) = N_0(x) \qquad \text{on } \Gamma, \tag{7}$$

$$\partial_t N([u],t) = \alpha\, e^{\left(\frac{[u](x,t)}{V_{ep}}\right)^2} \left(1 - \frac{N([u],t)}{N_0} e^{-q\left(\frac{[u](x,t)}{V_{\rm ep}}\right)^2}\right) \qquad \text{on } \Gamma\times]0,T[, \tag{8}$$

where α, β, q, and N_0 are constants, $V_{\rm ep}$ is the minimum transmembrane voltage for electropermeabilization, and T is the final time.

Given the condition

$$u(x,t) = u_{\rm ref} \qquad \text{on } Y \text{ for } t < 0, \tag{9}$$

the initial value problem (1)-(4) and (6)-(9) is then solved on $Y\times]0,T[$.

Another model for σ_m has been developed in [8]. Together with (6), (7), one uses the dynamics

$$\partial_t N([u],t) \quad = \max\left(\tfrac{\beta([u])-N([u],t)}{\tau_{\rm ep}}, \tfrac{\beta([u])-N([u],t)}{\tau_{\rm res}}\right) \tag{10}$$

with

$$\beta(\lambda) = (1+\tanh(k_{\rm ep}(|\lambda|-V_{\rm ep})))/2,$$

and given constants $\tau_{\rm ep}$, $\tau_{\rm res}$, and $k_{\rm ep}$.

3. Wellposedness of the electropermeabilization model

In this section, we treat the classical electropermeabilization model model (1)-(4) and (6)-(9) and study it in the form of an ODE on the membrane Γ.

As a preliminary step, let us prove the following representation of the pore density N.

Lemma 1. (i) *For $[u]=v$, the solution of the initial value problem in* (7), (8) *is*

$$N(x,t) = e^{-\int_0^t \frac{\alpha}{N_0}\, e^{(1-q)\left(\frac{v(x,\tau)}{V_{\rm ep}}\right)^2} d\tau}\, N_0 + \left(\int_0^t \alpha\, e^{\left(\frac{v(x,s)}{u_0}\right)^2} e^{-\int_s^t \frac{\alpha}{N_0}\, e^{(1-q)\left(\frac{v(x,\tau)}{V_{\rm ep}}\right)^2} d\tau}\, ds\right). \tag{11}$$

(ii) *The pore density N, considered as a mapping $v(x,t)\mapsto N(v(x,t),t)$*

$$C([0,T],C(\Gamma))\times[0,T]\to C([0,T],C(\Gamma)), \tag{12}$$

maps bounded sets to bounded sets.

Proof. Note that the solution to a linear inhomogeneous ordinary differential equation

$$\frac{\partial}{\partial t}N(t) = A(t)\,N(t) + b(t) \tag{13}$$

is given by [1, Thm. 5.14]

$$N(t) = U(t,0)\,N_0 + \int_s^t U(t,s)\,b(s)\,ds, \tag{14}$$

where

$$U(t,s) = \int_s^t A(\tau)\,d\tau.$$

Equation (8) is a special form of (13), and the coefficients A and b are

$$A(t) = -\frac{\alpha}{N_0}\, e^{(1-q)\left(\frac{[u](t)}{V_{\rm ep}}\right)^2},$$

and

$$b(t) = \alpha\, e^{\left(\frac{[u](t)}{V_{\rm ep}}\right)^2}.$$

Inserting A and b into the general solution (14), we directly obtain the representation (11) in (i).

Using the norm $\|v\|_{C(\Gamma)} = \sup_{x\in\Gamma}|v(x)|$, the boundedness property in (ii) is then immediate. □

Remark 1. In practice, it is clear that the potential v stays finite. One may therefore choose a real number $M > 0$ and work instead of $N(v,t)$ with the function

$$N_M(v,t) := N(v_M,t) \qquad \text{with } v_M := \begin{cases} |v| & |v| \le M \\ M & |v| > M \\ -M & |v| < M \end{cases}. \tag{15}$$

For $\|v\|_{L^\infty(\Gamma)} < M$, this cutoff preserves the pore density: $N_M(v,t) = N(v,t)$. In Lemma 3, it is shown that the function $v \mapsto N_M(v,t)v_M$, considered in $C((0,T);L^2(\Gamma))$, has a global Lipschitz property.

3.1. **Reduction to an ordinary differential equation.**

Definition 1 (Stekhlov-Poincaré operators)**.** *Let $H^s(\Gamma)$ be the standard Sobolev space on Γ of order s. Let $f \in H^{\frac{1}{2}}(\Gamma)$ be given. Define solutions of Dirichlet boundary value problems and assign the Neumann data via the* Stekhlov-Poincaré operators *Λ_c, Λ_e: $H^{1/2}(\Gamma) \to H^{-1/2}(\Gamma)$ and Λ_0: $H^{1/2}(\partial\Omega) \to H^{-1/2}(\Gamma)$,*

$$\Lambda_c f := \partial_n P_1, \quad \Lambda_e f := \partial_n P_2, \quad \Lambda_0 f := \partial_n P_3,$$

where $P_i, i = 1,2,3$ are solutions to

$$\begin{cases} \Delta P_1 = 0 & \text{in } Y_i, \\ P_1 = f & \text{on } \Gamma, \end{cases}$$

and

$$\begin{cases} \Delta P_2 = 0 & \text{in } Y_e, \\ P_2 = 0 & \text{on } \partial Y, \\ P_2 = f & \text{on } \Gamma, \end{cases} \qquad \begin{cases} \Delta P_3 = 0 & \text{in } Y_e, \\ P_3 = f & \text{on } \partial Y, \\ P_3 = 0 & \text{on } \Gamma. \end{cases}$$

The following results hold.

Lemma 2. (i) *Solving the problem* (1)-(4) *and* (6)-(9) *for $u = (u_i, v, u_e)$ on $Y_i \cup \Gamma \cup Y_e$ is equivalent to solving the initial value problem*

$$\begin{gathered} \frac{c_m}{\delta}\partial_t v + \frac{\sigma_m}{\delta}(v,t)v + \Lambda_c B^{-1} v = G, \\ v(0) = \varphi, \end{gathered} \tag{16}$$

for v on Γ, with the correspondence

$$\begin{aligned} u_i &= -B^{-1}(v + \Lambda_e^{-1}\Lambda_0 g), \\ u_e &= u_i + v. \end{aligned}$$

Here, $B = Id + \Lambda_e^{-1}\Lambda_0, G = -\Lambda_c B^{-1}\Lambda_e^{-1}\Lambda_0 g$, and

$$\sigma_m(v,t) = \sigma_{m0}(x) + \beta N(v,t). \tag{17}$$

(ii) *The linear operator $\Lambda_c B^{-1} : H^1(\Gamma) \to L^2(\Gamma)$ is m-accretive. In particular, one has*

$$\forall v : \qquad \langle \Lambda_c B^{-1} v, v\rangle_{L^2} \ge 0, \tag{18}$$

where $\langle\ ,\ \rangle_{L^2}$ is the scalar product on $L^2(\Gamma)$.

Proof. The reduction of the time-dependent model on Ω to the initial value problem on Γ in (16), using the Steklov-Poincaré operators, is the same as in [8, Lemma 9]. The property in (ii) is shown in [8, Lemma 8]. □

For establishing existence and uniqueness results (in Theorem 1), we use the following lemma on the Lipschitz property of the function N_M introduced in Remark 1.

Lemma 3. *Let $M > 0$, and let $N_M(v,t) = N(v_M,t)$ with $v_M = \operatorname{sgn}(v)\min(|v|, M)$ be the modified pore density defined by* (15)*. Then*

$$v \longmapsto N_M(v,t)v_M$$

is global Lipschitz in $C((0,T);L^2(\Gamma))$.

Proof. Let v_1, $v_2 \in C((0,T);L^2(\Gamma))$. One has the algebraic identity

$$N(v_{1M},t)v_{1M} - N(v_{2M},t)v_{2M} = \\ \big(N(v_{1M},t)v_{1M} - N(v_{1M},t)v_{2M}\big) + \big(N(v_{1M},t)v_{2M} - N(v_{2M},t)v_{2M}\big). \quad (19)$$

Using the boundedness of v_M, (19) shows that it suffices to prove that $N(v_M,t)$ is global Lipschitz in $C((0,T);L^2(\Omega))$.

Consider the explicit form of $N(v,t)$ in (11). As $\|v_M\|_{L^\infty} \le M$, there exists a constant $L(M)$ such that

$$|N(v_{1M},t) - N(v_{2M},t)|^2 \le L(M)\int_0^t |v_1(x,s) - v_2(x,s)|^2 ds. \quad (20)$$

Therefore, we have

$$\|N(v_{1M},t)v_{1M} - N(v_{2M},t)v_{2M}\|_{C((0,T);L^2(\Gamma))} \le C(M)\|v_1 - v_2\|_{C((0,T);L^2(\Gamma))}, \quad (21)$$

and the global Lipschitz property of N_M in $C((0,T);L^2(\Omega))$ holds. □

Using Lemma 3, we now come to the well-posedness results. For this end, we introduce the following auxiliary problem. As a variant to (4), we consider

$$\sigma(x)\mathbf{n}\cdot\nabla u(x,t) = \frac{c_m}{\delta}\partial_t[u](x,t) + \frac{\sigma_m\left([u]_M(x,t),t\right)}{\delta}[u]_M(x,t) \qquad \text{on } \Gamma. \quad (4')$$

Using the same procedure as in Lemma 2, we find that the model (1)-(3),(4') and (6)-(9) is equivalent to solving

$$\frac{c_m}{\delta}\partial_t\tilde{v} + \frac{\sigma_m(\tilde{v}_M,t)}{\delta}\tilde{v}_M + \Lambda_c B^{-1}\tilde{v} = G, \\ \tilde{v}(0) = \varphi. \quad (22)$$

Let us now state the well-posedness properties of our initial value problems on Γ.

Theorem 1. *Let $G \in C^1((0,T);H^1(\Gamma))$ and $\varphi \in H^2(\Gamma)$.*

(i) *The initial value problem in* (22) *has a unique global solution $\tilde{v} \in C([0,T];H^2(\Gamma))$.*
(ii) *For the initial value problem* (16)*, there is a $t_0 > 0$ such that there exists a solution $v \in C([0,t_0[;H^2(\Gamma))$.*
(iii) *The solution in (ii) is unique on $C([0,t_1],H^2(\Gamma))$ for any closed interval $[0,t_1] \subset [0,t_0[$.*

Proof. (i): Let $M > \|\varphi\|_{L^\infty}$ be a constant and consider the initial value problem (22). Fix a number $T > 0$.

Due to the global Lipschitz property of $N_M v_M$ shown in Lemma 3, one can apply the fixed point argument in [8, Thm.10]) to conclude that there exists a unique solution $\tilde{v} \in C([0,T]; L^2(\Gamma))$ solving (22).

If one additionally assumes that $G \in C^1([0,T]; H^1(\Gamma))$ and $\varphi \in H^2(\Gamma)$, then one can likewise conclude $\tilde{v} \in C^1([0,T]; H^2(\Gamma))$. Then we have that $\partial_n u_i \in L^2(\Gamma)$. With such boundary regularity, we infer $\tilde{u}_i \in H^{3/2}(Y_i)$, similarly $\tilde{u}_e \in H^{3/2}(Y_e)$. Then $\tilde{v} = \tilde{u}_e - \tilde{u}_i \in C([0,T]; H^1(\Gamma))$. Using this argument once again, we have that $\tilde{v} = \tilde{u}_e - \tilde{u}_i \in C([0,T]; H^2(\Gamma))$.

(ii): We will now show that the solution $\tilde{v}$ to (22) found in point (i) solves locally the original problem (16). – Using the Sobolev embedding theorem one has that

$$\Lambda_c B^{-1} \tilde{v} \in C([0,T]; H^1(\Gamma)) \hookrightarrow C([0,T]; C(\Gamma)).$$

Take a constant C_M such that, for any $t \leq T$, one has

$$\left\| \frac{\sigma_m(\tilde{v}_M, t)}{\delta} \tilde{v}_M + \Lambda_c B^{-1} \tilde{v} + G \right\|_{C(\Gamma)} \leq C_M.$$

Define

$$t_0 := \frac{c_m}{\delta} \frac{M - \|\varphi\|_{L^\infty}}{C_M}.$$

Then, for $t \leq t_0$, one gets

$$\begin{aligned} \|\tilde{v}(x,t)\|_{L^\infty(\Gamma)} &\leq \|\varphi\|_{L^\infty} + tC_M, \\ &\leq M. \end{aligned}$$

But for $\|\tilde{v}\|_\infty < M$, one has that $\tilde{v}_M = \tilde{v}$ and $N_M(\tilde{v}, t) = N(\tilde{v}, t)$. Therefore, the expressions in (16) and (22) are the same, which implies that, locally, $\tilde{v}$ solves as well the original initial value problem (16).

(iii): Take two solutions v, w to (16) in $C^1([0,t_1], H^2(\Gamma))$. Due to closedness of $[0,t_1]$ and continuity of the norm $\|.\|_{H^2} \to \mathbb{R}$, there exists a $M > 0$ such that for every $t \in [0,t_1]$, one has

$$\|v(t)\|_{H^2} < M \qquad \text{and} \qquad \|w(t)\|_{H^2} < M.$$

But then the cutoff with respect to M does not change the functions: $v_M = v$ and $w_M = w$. Therefore, v and w also solve (22). But for that ODE, one has a global uniqueness property. Therefore $v = w$ on $[0,t_1]$. □

We now give a more detailed analysis of the terms in equation (16) to show that a solution cannot blow up in finite time (see Theorem 2).

Note that for σ_m given by (6), there exists a $C \in \mathbb{R}$ such that one has for all v that

$$\langle \sigma_m(v,t)v, v \rangle_{L^2} \geq C \|v\|^2_{L^2}. \tag{23}$$

This immediately follows from the expression of the membrane conductivity in (6) and the fact that both the pore density N as well as N_M in (15) are positive.

Theorem 2. *For a function $v \in C^1([0,t_0[, L^2(\Gamma))$ which solves (16), it is impossible that*

$$\|v(t_k)\|_{L^2(\Gamma)} \longrightarrow_{t \to b} \infty \qquad \textit{for } b \in [0,t_0[.$$

Proof. Take as an indirect assumption a blow up-sequence $\|v(t_k)\|_X \to \infty$ with $t_k \to b$. Without loss of generalization, we may choose $t_k \in [0, t_0[\cap W$, where W is a neighborhood of b such that v is nonzero on $[0, t_0[\cap W$. Due to the C^1-regularity property of $v(t)$ and $v \neq 0$, the function

$$[0, t_0[\cap W \to \mathbb{R} : \qquad t \longmapsto \|v(t)\|_{L^2}$$

is then continuously differentiable.

The sequence $t_k \to b(x)$ having the Cauchy property, the slope of the secants satisfies

$$\frac{|\|v(t_{k+1})\|_- \|v(t_k)\||}{t_{k+1} - t_k} \longrightarrow \infty,$$

as well. We then will work with a sequence τ_k such that

$$\partial_t \|v(\tau_k)\|_{L^2} \longrightarrow \infty, \tag{24}$$

chosen by the mean-value theorem.

Consider equivalently to (16) the equation

$$\sigma(v)v = G - C_m \partial_t v - \Lambda_c B^{-1} v.$$

Take the L^2-scalar product with v and take account of $\langle \partial_t v, v\rangle = \|v\|\ \partial_t \|v\|$. Then estimate the right-hand side with the Cauchy-Schwarz inequality and the accretivity property (18):

$$\begin{aligned} \langle \sigma(v)v, v\rangle_{L^2} &= \langle G, v\rangle_{L^2} - C_m \langle \partial_t v, v\rangle_{L^2} - \langle \Lambda_c B^{-1} v, v\rangle_{L^2}, \\ &\leq \|G\|_{L^2} \|v\|_{L^2} - C_m \|v\|_{L^2}\ \partial_t \|v\|_{L^2}. \end{aligned}$$

Divide by $\|v\|_{L^2}$ to find

$$\frac{\langle \sigma(v)v, v\rangle_2}{\|v\|_{L^2}} \leq \|G\|_{L^2} - C_m \partial_t \|v\|_{L^2}. \tag{25}$$

From (23), we already know that the left-hand side stays positive.

Evaluate then expressions in inequality (25) for the sequence τ_k in (24). The result is that the right-hand side would tend to $-\infty$, which is impossible. This shows that no blow up of v in L^2 can occur. □

4. Homogenization

Let Ω be a bounded domain in $\mathbb{R}^2$, which carries a periodic structure made up by periodic open sets εY. The reference domain $Y = Y_i \cup Y_e \cup \Gamma$ contains a cell inside with membrane Γ, where Y_i is the intracellular domain and Y_e is the extracellular domain. The whole domain Ω is thus composed of

$$\Omega = \Omega^+ \cup \Omega^- \cup \Gamma_\varepsilon,$$

where Ω^+ is the collection of extracellular domains, Ω^- is the collection of intracellular domains and Γ_ε is the collection of membranes.

We write the thickness of the membrane of the cells εY in the form

$$\delta = \varepsilon\ \delta_0,$$

where ϵ is the scale of the cell and δ_0 is the reference cell membrane thickness for Y.

As in [3], we want to study behavior of the electrical field on this cell cluster and recover features of the microscopic cell model from tissue measurements. Considering the cell model in (1)-(4) and (6)-(9) for a domain Y, we first give the model equation for u_ε in Ω:

$$\begin{aligned} \nabla \cdot (\sigma(x)\nabla u_\varepsilon(x,t)) &= 0 && \text{in } \Omega^+, \\ \nabla \cdot (\sigma(x)\nabla u_\varepsilon(x,t)) &= 0 && \text{in } \Omega^-, \\ [\sigma \nabla u_\varepsilon \cdot \mathbf{n}] &= 0 && \text{on } \Gamma_\varepsilon, \\ \frac{c_m}{\delta}\frac{\partial}{\partial t}[u_\varepsilon] + \frac{1}{\delta}\sigma_m([u_\varepsilon]_M, t)[u_\varepsilon]_M &= \sigma \partial_n u_\varepsilon^- && \text{on } \Gamma_\varepsilon, \\ [u_\varepsilon](x,0) &= S_\varepsilon && \text{on } \Gamma_\varepsilon, \\ u_\varepsilon(x,t) &= 0 && \text{on } \partial\Omega, \end{aligned} \tag{26}$$

where $S_\varepsilon(x) = \varepsilon S_1(x, \frac{x}{\varepsilon}) + R(\varepsilon)$ and $\sigma_m = \sigma_{m0} + \beta N([u_\varepsilon], t)$. The pore density $N([u_\varepsilon], t)$ is governed by (8).

Here, in the second equation on Γ_ε, the quantity $[u_\varepsilon]_M$ is understood in the sense of the definition in (15), i.e., $[u_\varepsilon]_M = \operatorname{sgn}([u_\varepsilon]) \min(|[u_\varepsilon]|, M)$ for a constant $M > 0$.

Given the physical observation that the voltage v stays bounded, it is reasonable that for proper $M > 0$, the system (26) is an accurate model for the real potential. Given Lemma 2 and Theorem 1, it is also well-posed.

We want to explore the limit of the solution u_ε as $\varepsilon \to 0$. For this end, we start with an energy estimate on the solution u_ε which will be needed later when investigating the limit.

Proposition 1. (i) *We have for u_ε in (26) the energy estimate*

$$\int_0^t \int_\Omega \sigma |\nabla u_\varepsilon|^2 dx\, dt + \frac{1}{\varepsilon}\int_{\Gamma_\varepsilon} [u_\varepsilon]^2(x,t) dS \le C. \tag{27}$$

(ii) *In particular, the estimate*

$$\int_{\Gamma_\varepsilon} [u_\varepsilon]^2 dS \le C\varepsilon \tag{28}$$

holds.

Proof. Multiply (26) by u_ε, then integrate by parts to find

$$\begin{aligned} &\int_0^t \int_\Omega \sigma |\nabla u_\varepsilon|^2 dx\, dt + \frac{\alpha}{2\varepsilon}\int_{\Gamma_\varepsilon} [u_\varepsilon]^2(x,t) dS \\ &\qquad + \frac{1}{\varepsilon}\int_0^t \int_{\Gamma_\varepsilon} \sigma_m([u_\varepsilon]_M, \tau)[u_\varepsilon][u_\varepsilon]_M(x,t) dS\, dt = \frac{\alpha}{2\varepsilon}\int_{\Gamma_\varepsilon} [S_\varepsilon]^2(x) dS. \end{aligned} \tag{29}$$

The statement is then derived from the fact that

$$\sigma_m [u_\varepsilon][u_\varepsilon]_M \ge 0$$

and $S_\varepsilon(x) = \varepsilon S_1(x, \frac{x}{\varepsilon}) + o(\varepsilon)$. □

For now, let us formally assume that the solution u_ε of (26) has the form

$$u_\varepsilon(x,t) = u_0(x,t) + \varepsilon u_1(x, \frac{x}{\varepsilon}, t) + o(\varepsilon). \tag{30}$$

We will calculate the equation for u_0 in Subsection 4.1 and then prove rigorously that u_ε converges in an appropriate sense to u_0 in Subsection 4.2.

4.1. **Formal calculation of the homogenization limit.** To find the precise form of the terms in the ansatz (30), we can apply the arguments developed in [2]. For this end, it is required that for the membrane conductivity one has that

$$\sigma_m(0,t) = \text{constant}.$$

(see [2, Secs. 3.2 and 3.3]). This condition can be ensured for the model (6), together with (8): From (11), one can prove that $N(0,t) = N_0$, and therefore $\sigma_m(0,t) = \text{constant}$.

Before calculating the limit, we first give some definitions. Introduce the transform

$$T : H^{1/2}(\Gamma) \to C([0,T], H^1_p(Y)),$$

where

$$H^1_p(Y) = \left\{ u \textit{ is periodic in } Y : u|_{Y_i} \in H^1(Y_i) \text{ and } u|_{Y_e} \in H^1(Y_e), \ \int_Y u = 0 \right\},$$

by

$$T(s)(y,t) := v(y,t)$$

with v being the solution to the following system with boundary data s:

$$\begin{aligned}
\nabla \cdot (\sigma(x)\nabla v) &= 0 && \text{in } Y_i,\\
\nabla \cdot (\sigma(x)\nabla v) &= 0 && \text{in } Y_e,\\
[\sigma \nabla v \cdot \mathbf{n}] &= 0 && \text{on } \Gamma,\\
\frac{c_m}{\delta_0}\frac{\partial}{\partial t}[v] + \frac{1}{\delta_0}\sigma_m(0,t)[v] &= \sigma \partial_n v^- && \text{on } \Gamma,\\
[v](x,0) &= s && \text{on } \Gamma.
\end{aligned}$$

We define next the cell problems $\chi^0 : \Omega \to \mathbb{R}^d$ and $\chi^1 : \Omega \times (0,T) \to \mathbb{R}^d$. For this, let $\mathbf{e}_h$ be the h-th unit vector in $\mathbb{R}^d$. Then the component $\chi^0_h \in H^1_p(Y)$ satisfies

$$\begin{aligned}
\nabla \cdot (\sigma(x)\nabla \chi^0_h) &= 0 && \text{in } Y_i,\\
\nabla \cdot (\sigma(x)\nabla \chi^0_h) &= 0 && \text{in } Y_e,\\
[\sigma(\nabla_y \chi^0_h - \mathbf{e}_h) \cdot \mathbf{n}] &= 0 && \text{on } \Gamma,\\
[\chi^0_h](x,0) &= 0 && \text{on } \Gamma.
\end{aligned}$$

The component χ^1_h is defined by

$$\chi^1_h = T(\sigma(\nabla_y \chi^0_h - \mathbf{e}_h) \cdot \mathbf{n}). \tag{31}$$

By a calculation analogous to [2, Sec.3], one finds that the candidate u_0 in equation (30) satisfies

$$\operatorname{div}\left[-\sigma_0\nabla_x u_0 - A^0\nabla_x u_0 - \int_0^t A^1(t-\tau)\nabla_x u_0(x,\tau)d\tau + \mathbf{F}(x,t)\right] = 0. \tag{32}$$

Here, the matrices A^0, A^1, and $\mathbf{F}(x,t)$ are defined by

$$\begin{cases} \sigma_0 = \sigma_1|Y_i| + \sigma_2|Y_e|, \\ (A^0)_{jh} = \displaystyle\int_\Gamma [\sigma]\chi_h^0 n_j dS, \\ (A^1)_{jh} = \displaystyle\int_\Gamma [\sigma\chi_h^1] n_j dS, \\ \mathbf{F} = \displaystyle\int_\Gamma [\sigma T(S_1(x,\cdot))](y,t)\ \mathbf{n}\ dS, \end{cases} \tag{33}$$

where $\sigma_i = \sigma|_{Y_i}$ and $\sigma_e = \sigma|_{Y_e}$, with χ_h^0, χ_h^1 and T given above.

4.2. **Convergence.** While in Subsection 4.1, we derived the formal limit (32) for the ansatz of the asymptotic expansion (30), we now state its convergence properties.

Theorem 3. *For the periodic solution u_ε in (26) and the homogenized solution u_0 in (32), we have the convergence*

$$u_\varepsilon \to u_0$$

weakly in $L^2([0,T]\times\Omega)$ and strongly in $L^1_{\mathrm{loc}}([0,T],\Omega)$.

The proof relies on arguments developed in [2]. For the sake of a readability, we outline them in the appendix, and only prove here the crucial lemma needed for their adaption to our case.

Lemma 4. *For $M > 1$, there exists a constant $C(M)$ such that*

$$\int_0^T \int_{\Gamma_\varepsilon} |\sigma_m(0,t)[u_\varepsilon] - \sigma_m([u_\varepsilon]_M, t)\ [u_\varepsilon]_M\ dS\ |dt \le C\varepsilon. \tag{34}$$

Proof. We have

$$\begin{aligned} & \sigma_m(0,t)[u_\varepsilon] - \sigma_m([u_\varepsilon]_M,t)\ [u_\varepsilon]_M & (35)\\ = \ & \sigma_m(0,t)[u_\varepsilon] - \sigma_m([u_\varepsilon]_M,t)\ [u_\varepsilon] + \sigma_m([u_\varepsilon]_M,t)\ ([u_\varepsilon] - [u_\varepsilon]_M). & (36)\end{aligned}$$

By the explicit form of $N(v,t)$ in (11) and $|v_M|_{L^\infty} \le M$, there exists a constant $L(M)$ such that

$$|N([u_\varepsilon]_M,t) - N(0,t)|^2 \le L(M)\int_0^t [u_\varepsilon]_M^2 ds, \tag{37}$$

and $\sigma_m([u_\varepsilon]_M,t) \le C(M)$.

Together with the fact that $\left|\int_0^T [u_\varepsilon] - [u_\varepsilon]_M\ ds\right| \le \int_0^T [u_\varepsilon]^2 ds$, we can thus conclude that

$$\int_0^T \int_{\Gamma_\varepsilon} \left|\sigma_m(0,t)[u_\varepsilon] - \sigma_m([u_\varepsilon]_M,t)\ [u_\varepsilon]_M\right| dS\ dt \le C(M)\varepsilon.$$

The lemma then follows by the energy estimate (28). □

Symbol	Value	Definition
σ_i	0.455	intracellular conductivity
σ_e	5	extracellular conductivity
L	2×10^{-4}	computation domain size
r	0.5×10^{-4}	cell radius
δ	5×10^{-9}	membrane thickness
r_p	0.76	pore radius
σ_p	0.0746	pore conductivity
V_{ep}	0.258	characteristic voltage of electropermeabilization
α	10^9	electropermeabilization parameter
N_0	1.5×10^9	equilibrium pore density
c_m	9.5×10^{-12}	membrane capacitance

TABLE 1. Model parameters used for the numerical computations.

5. Numerical experiments

In the preceding section, we have modeled macroscopic processes as homogenized quantities with specific effective material parameters. In this section we show the sensitivity of the effective parameters to microscopic properties relevant in electropermeabilization.

We use FEM with mesh generator [17] to implement all the numerical simulations. We present the numerical experiments from two aspects: First we will simulate the single cell model (16) and show the electropermeabilization at cell level. Next we show how the microscopic parameters affect effective parameters and anisotropy properties in the homogenized model (32).

5.1. **Electropermeabilization simulation for a single cell.** We simulate the single cell model (16) in a square domain $[0, L] \times [0, L]$, the cell is a circular in the center of the square with cell radius r. The parameter β in (8) is given by

$$\beta = \frac{2\pi r_p^2 \sigma_p \delta}{\pi r_p + 2\delta}. \tag{38}$$

All the parameters are given in Table 1. Figure 1 shows the results for the time evolution and the voltage after 2 $\mu s'$.

5.2. **Homogenization for electropermeabilization model.** In this section, we show the sensitivity of the effective parameters σ_0, A^0, and A^1 in (32) to

- the conductivities σ_o and σ_i;
- the shape of the cell with membrane Γ;
- the volume fraction $f = \frac{\text{vol}(Y_i)}{\text{vol}(Y)}$;
- the lattice of the cells in the domain Ω.

We perform four experiments, the results of which are found in Table 2.

Example 1. We fix the shape and size of the cell and change the ratio of the interior and exterior conductivities σ_i and σ_e.

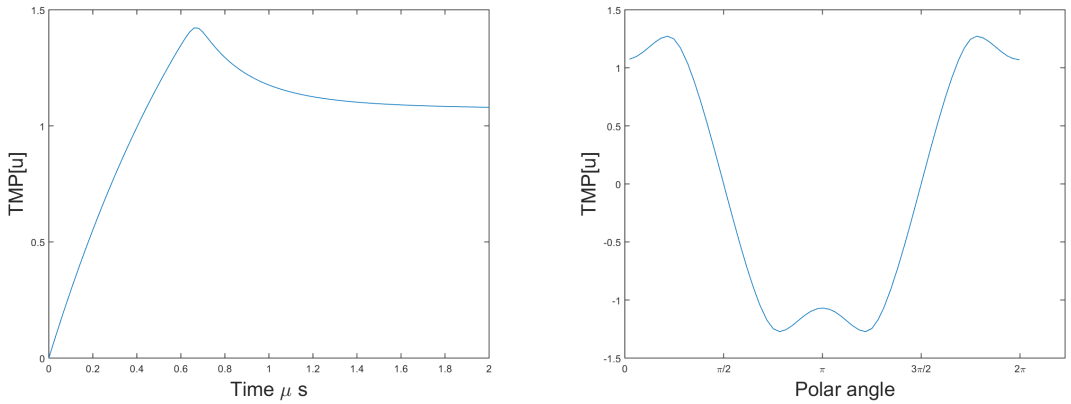


FIGURE 1. **(a)** Evolution of the transmembrane potential (TMP) v at the pole of the cell. **(b)** TMP along the cell membrane after 2 $\mu s'$.

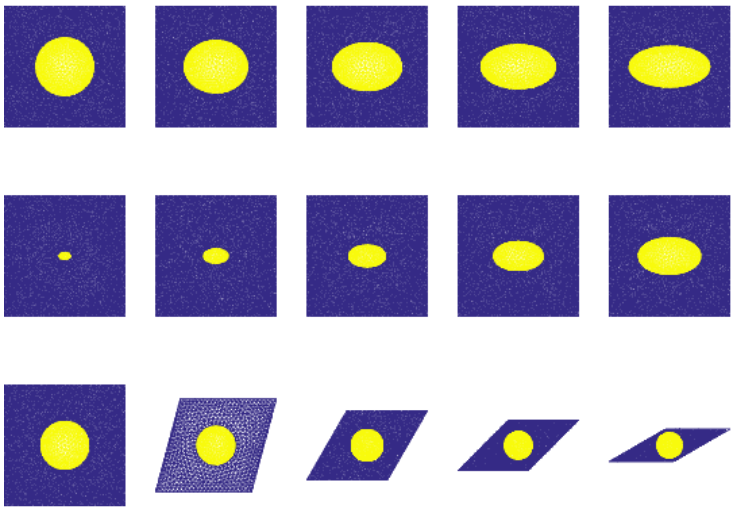


FIGURE 2. Cell shapes used in numerical examples (see text and Table 2). Example 1 uses the first mesh. Example 2 uses the cells in the first row. Example 3 uses the cells in the second row. Example 4 uses the cells in the last row.

Example 2. In this example, we show how the shape of the cell membrane produces different effective anisotropy properties. We fix conductivities and the volume fraction of the cell, but take as cell shapes ellipses with different excentricity a/b.

Example 3. We investigate the effect of different volume fractions of a cell with the same shape.

Example 4. In this example, we show how the angle of the lattice in which the cells are arranged affects the effective parameters.

For all these experiments, Table 2 presents the reactions of the effective conductivity σ_0 and the effective anisotropy properties A^0 and $A^1(0)$ to the microscopical change. One sees clearly that σ_0, as well as A^0 and A^1 react to a change of cell and conductivity parameters. Most of the sensitivity functions are in fact monotonic.

The best contrast is seen in:

- the reaction of σ_0 to the change in conductivity σ_i/σ_e and to a change in the lattice angle ϕ;
- the reaction of both A^0 and A^1 to the cell shape.

The volume fraction alone does not show so much contrast in the anisotropy of the effective parameters.

Given the results of the sensitivity analysis, it is promising to infer shape parameters from macroscopic effective properties in electropermeabilization, as it was done in [3] from multifrequency admittivity measurements.

6. Concluding remarks

We introduced a homogenization scheme relating critical microscopic and macroscopic quantities in electropermeabilization. The sensitivity analysis of the effective parameters showed this dependence and opens the door to solve the inverse problem to monitor those critical microscopic quantities in practice.

While setup optimization for electropermeabilization has been studied using computer simulations, for instance, in [12, 20, 5, 13, 11], from our approach comes an additional constraint: for mapping of the effective parameters A^1 and A^0, two currents have to be applied which are nowhere parallel. An electrode configuration providing this allows for unique reconstruction [9].

Appendix A. Convergence for homogenization

We give here the outline of the method used in [2]. It shows how Lemma 4 is used to prove Theorem 3 for our application.

Theorem 4. *For the solution u_ε in* (26) *and the homogenized solution u_0 in* (32)*, we have the convergence*

$$u_\varepsilon \to u_0$$

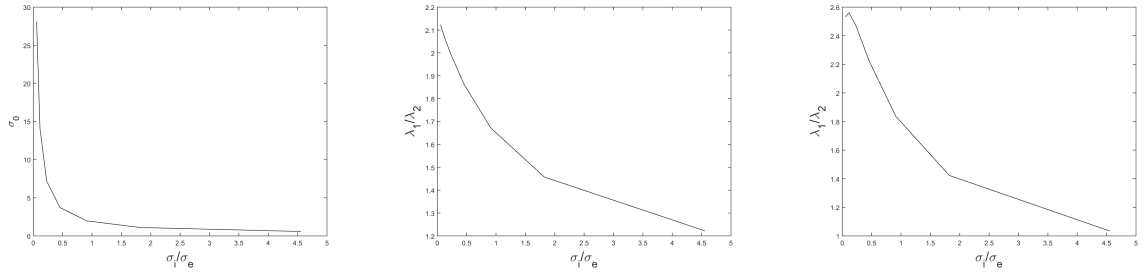
weakly in $L^2([0,T]\times\Omega)$ and strongly in $L^1_{\mathrm{loc}}([0,T],\Omega)$.

Proof. From the estimate (27) we get, extracting subsequences if needed

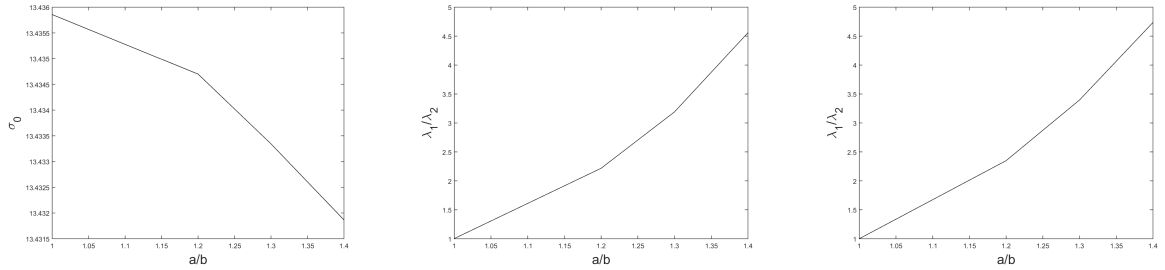
$$\begin{aligned} &u_\varepsilon \to u_0, \qquad \sigma\nabla u_\varepsilon \to \xi \qquad && \text{weakly in } L^2([0,T]\times\Omega),\\ &u_\varepsilon \to u_0 && \text{strongly in } L^1_{\mathrm{loc}}([0,T],\Omega). \end{aligned} \tag{39}$$

effective conductivity σ_0	eigenvalues λ_1/λ_2 of A^0	eigenvalues λ_1/λ_2 of $A^1(0)$.

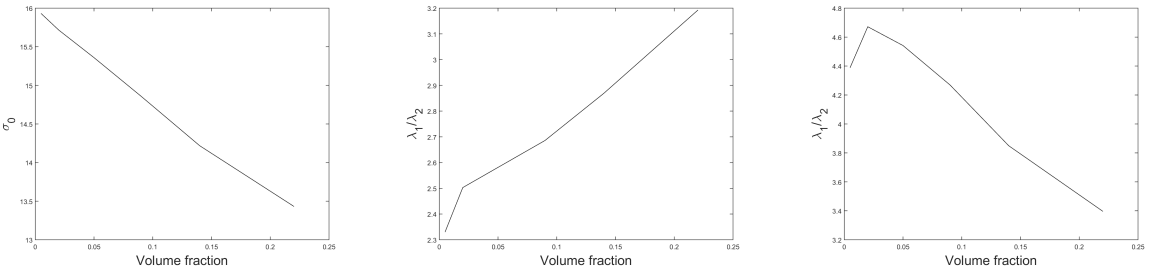
Example 1: Difference in conductivity (ratio σ_i/σ_e of interior and exterior conductivity).



Example 2: Difference in cell shape: change of the excentricity a/b (see Fig. 2, 1st row).



Example 3: Difference in volume fraction of the cells (see Fig. 2, 2nd row).



Example 4: Difference in angle ϕ of the lattice arrangement (see Fig. 2, 3rd row).

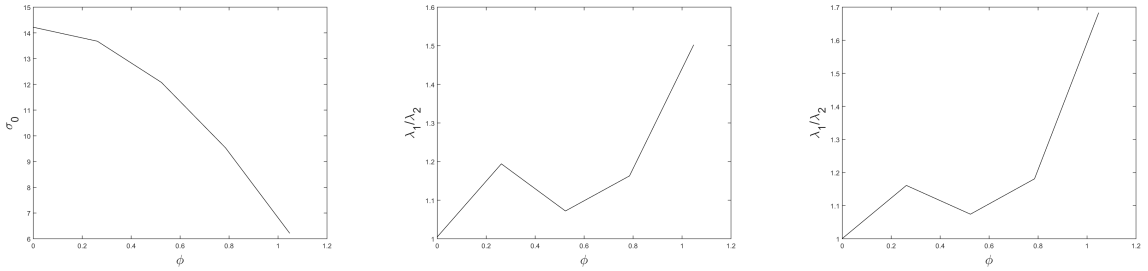


TABLE 2. Changes in microscopic parameters and the reaction of the effective parameters in (32).

Next, consider the weak formulation of system (26):

$$\begin{aligned}\int_0^T \int_\Omega \sigma \nabla u_\varepsilon \cdot \nabla \psi \; dx \; dt + \frac{1}{\varepsilon} \int_0^T \int_{\Gamma_\varepsilon} \sigma_m([u_\varepsilon]_M)[u_\varepsilon]_M[\psi] \; dS \; dt \\ -\frac{c_m}{\delta} \int_0^T \int_{\Gamma_\varepsilon} [u_\varepsilon] \frac{\partial}{\partial t}[\psi] \; dS \; dt - \frac{c_m}{\delta} \int_{\Gamma\varepsilon} [u_\varepsilon](0)[\psi](0) \; dS = 0.\end{aligned} \tag{40}$$

The general idea is to pass to the limit $\varepsilon \to 0$ in this equation, and therefore to obtain the equation for u_0. This is possible for special test functions ψ.

Choose for ψ the functions $\varphi \; w_h^\varepsilon(x,t)$ for $h = 1, \ldots, d$, where φ is a smooth with compact support on Ω, and w_h^ε is built by the cell functions χ^1 and χ^2:

$$w_h^\varepsilon(x,t) := x_h - \varepsilon \chi_h^0 \left(\frac{x}{\varepsilon} - \varepsilon \right) \int_t^T \chi_h^1 \left(\frac{x}{\varepsilon}, \tau - t \right) \; d\tau.$$

For this definition, given in [2, (5.1)] one has the weak formulation in [2, (5.2)-(5.4)].

By subtracting the weak equation (40) for $\psi = w_h^\varepsilon(x,t)$ and the equations [2, (5.2)-(5.4)], one can isolate the term $\int \int \sigma \nabla u_\varepsilon \nabla \varphi w_h^\varepsilon \; dx \; dt$:

$$\int_0^T \int_{\Gamma_\varepsilon} \sigma \nabla u_\varepsilon \nabla \varphi w_h^\varepsilon \; dx \; dt = K_{1\varepsilon} + K_{2\varepsilon} + K_{3\varepsilon}, \tag{41}$$

with

$$\begin{aligned} K_{1\varepsilon} &= \int_0^T \int_{\Gamma_\varepsilon} \sigma \nabla w_h^\varepsilon \nabla \varphi u_\varepsilon \; dx \; dt, \\ K_{2\varepsilon} &= -c_m \varepsilon \int_{\Gamma_\varepsilon} (S_1(x, \frac{x}{\varepsilon}) + R_\varepsilon) \varphi \int_0^T [\chi_h^2](\frac{x}{\varepsilon}, \tau) d\tau dS, \\ K_{3\varepsilon} &= \frac{1}{\varepsilon} \int_0^T \int_{\Gamma_\varepsilon} \Big(\sigma_m(0,t)[u_\varepsilon] - \sigma_m([u_\varepsilon], t)[u_\varepsilon] \Big) [w_h^\varepsilon] \varphi \; dS \; dt. \end{aligned} \tag{42}$$

The limits of $K_{1\varepsilon}$ and $K_{2\varepsilon}$ are the same as in [2, p.18], whereas for the limit $K_{3\varepsilon}$, one can show that $K_{3\varepsilon} \to 0$ by Lemma 4. One can take then the limit $\varepsilon \to 0$ in (41) in order to obtain information on the specific form of the limit u_0 in (39). We get

$$\begin{aligned} -\int_0^T \int_\Omega \xi \cdot \nabla \varphi x_h \; dx \; dt = \int_0^T \int_\Omega \varphi(x) F_h(x,\tau); dx \; d\tau \\ + \int_0^T \int_\Omega u_0(x,t)(\sigma_0 I + A^0)\mathbf{e}_h + \int_0^t u_0(x,\tau) A^1(t-\tau)\mathbf{e}_h \; d\tau \cdot \nabla \varphi(x) \; dx \; dt \end{aligned} \tag{43}$$

with A^0, A^1, $\mathbf{F}$ defined as in (33). Choosing $\psi = \varphi \; x_h$ in (40), combining with (43), and differentiating in T gives then expressions which show that $u_0 \in L^2([0,T], H^1(\Omega))$ and that actually (32) is the correct equation of the limit u_0.

□

References

[1] H. Amann. *Ordinary differential equations. An introduction to nonlinear analysis.* de Gruyter Studies in Mathematics. Walter de Gruyter, Berlin, New York, 1990.

[2] M. Amar, D. Andreucci, P. Bisegna, and R. Gianni. Evolution and momory effects in the homogenization limit for electrical conduction in biological tissues. *Math. Models Methods Appl. Sci.*, 14(09):1261–1295, 2004.
[3] H. Ammari, J. Garnier, L. Giovangigli, W. Jing and J.K. Seo, Spectroscopic imaging of a dilute cell suspension, J. Math. Pure Appl., doi:10.1016/j.matpur.2015.11.009.
[4] J. Dermol and D. Miklavčič. Predicting electroporation of cells in an inhomogeneous electric field based on mathematical modeling and experimental CHO-cell permeabilization to propidium iodide determination. *Bioelectrochemistry*, 100:52–61, 2014.
[5] A. Golberg and B. Rubinsky. Towards electroporation based treatment planning considering electric field induced muscle contractions. *Technol. Cancer. Res. Treat.*, 11(2):189–201, 2012.
[6] A. Ivorra. Tissue electroporation as a bioelectric phenomenon: Basic concepts. In B. Rubinsky, editor, *Irreversible Electroporation*, Series in Biomedical Engineering, pages 23–61. Springer, Berlin, Heidelberg, 2010.
[7] A. Ivorra, J. Villemejane, and L. M. Mir. Electrical modeling of the influence of medium conductivity on electroporation. *Phys. Chem. Chem. Phys.*, 12:10055–10064, 2010.
[8] O. Kavian, M. Leguèbe, C. Poignard, and L. Weynans. "Classical" electropermeabilization modeling at the cell scale. *J. Math. Biol.*, 68:235–265, 2014.
[9] Y. J. Kim, O. Kwon, J. K. Seo, and E. J. Woo. Uniqueness and convergence of conductivity imge reconstruction in magnetic resonance electrical impedance tomography. *Inverse Probl.*, 19:1213–1225, 2003.
[10] M. Kranjc, B. Markelc, F. Bajd, M. Čemažar, I. Serša, T. Blagus, and D. Miklavčič. In situ monitoring of electric field distribution in mouse tumor during electroporation. *Radiology*, 274(1):115–123, 2015.
[11] D. Miklavčič, K. Beravs, D. Šemrov, M. Čemačar, F. Demsar, and G. Serša. The importance of electric field distribution for effective in vivo electroporation of tissues. *Biophys. J.*, 74:2152–5158, 1998.
[12] D. Miklavčič, M. Snoj, A. Zupanic, B. Kos, M. Čemažar, M. Kropivnik, M. Bracko, T. Pecnik, E. Gadzijev, and G. Serša. Towards treatment planning and treatment of deep-seated solid tumors by electrochemotherapy. *Biomed. Eng. Online*, 9(10), 2010.
[13] D. Miklavčič, D. Šemrov, H. Mekid, and L. M. Mir. A validated model of in vivo electric field distribution in tissues for electrochemotherapy and for DNA electrotransfer for gene therapy. *Biochim. Biophys. Acta*, 1523:73–83, 2000.
[14] J. C. Neu and W. Krassowska. Asymptotic model of electroporation. *Phys. Rev. E*, 59(3):3471–3482, 1999.
[15] M. Pavlin, N. Pavšelj, and D. Miklavčič. Dependence of induced transmembrane potential on cell density, arrangement and cell position inside a cell system. *IEEE Trans. Biomed. Eng.*, 49(6):605–612, 2002.
[16] M. Pavlin, T. Slivnik, and D. Miklavčič. Effective conductivitiy of cell suspensions. *IEEE Trans. Biomed. Eng.*, 49(1):77–80, 2002.
[17] P.-O. Persson and G. Strang. A simple mesh generator in MATLAB. *SIAM Rev.*, 46(2):329–345, 2004.
[18] G. Pucihar, T. Kotnik, B. Valič, and D. Miklavčič. Numerical determination of transmembrane voltage induced on irregularly shaped cells. *Ann. Biomed. Eng.*, 34(4):642–652, 2006.
[19] J.K. Seo and E.J. Woo, Magnetic resonance electrical impedance tomography (MREIT), SIAM Rev., 53 (2011), 40–68.
[20] K. Sugibayashi, M. Yoshida, K. Mori, T. Watanabe, and T. Hasegawa. Electric field analysis on the improved skin concentration of benzoate by electroporation. *Int. J. Pharm.*, 219:107–112, 2001.
[21] L. Towhidi, Kotnik. T., G. Pucihar, S. M. P. Firoozabadi, H. Mozdarani, and D. Miklavčič. Variability of the minimal transmembrane voltage resulting in detectable membrane electroporation. *Electromagn. Biol. Med.*, 27:372–385, 2008.

Department of Mathematics, ETH Zürich, Rämistrasse 101, CH-8092 Zürich, Switzerland
E-mail address: habib.ammari@math.ethz.ch

Department of Mathematics and Applications, Ecole Normale Supérieure, 45, rue d'Ulm, 75230 Paris Cedex 05, France
E-mail address: thomas.widlak@ens.fr

Department of Mathematics and Applications, Ecole Normale Supérieure, 45, rue d'Ulm, 75230 Paris Cedex 05, France
E-mail address: wenlong.zhang@ens.fr